Magnetoelectric Coupling in Self-Assembled $BiFeO_3$-$CoFe_2O_4$ Nanocomposites on (110)-$LaAlO_3$ Substrates

Zhuhua Mo,[1] Guo Tian,[1,2,*] Wenda Yang,[1] Shuai Ning,[2] Caroline A. Ross,[2,*] Xingsen Gao,[1,*] and Junming Liu[1,3]

[1]Guangdong Provincial Key Laboratory of Quantum Engineering and Quantum Materials, Institute for Advanced Materials, South China Academy of Advanced Optoelectronics, South China Normal University, Guangzhou 510006, China
[2]Department of Materials Science and Engineering, Massachusetts Institute of Technology, Cambridge, MA 02139, USA
[3]Laboratory of Solid-State Microstructures and Innovation Center of Advanced Microstructures, Nanjing University, Nanjing 210093, China

ABSTRACT

We describe the magnetic domain structures and magnetoelectric coupling in self-assembled $BiFeO_3$-$CoFe_2O_4$ (BFO-CFO) nanocomposite thin films grown on (110)-$LaAlO_3$ substrates, consisting of CFO slab-shaped crystals (nanofins) embedded in a BFO matrix. The nanofins exhibit magnetic single-domain states with in-plane magnetization along their length due to shape and magnetoelastic anisotropy. The piezoresponse of the BFO matrix is affected by applying an in-plane hard axis magnetic field, indicating magnetoelectric coupling within the multiferroic composite. Conversely, an applied electric field leads to magnetic reversal of a fraction of the nanofins as strain transferred from the BFO alters the magnetic anisotropy, enabling switching driven by magnetostatic interactions.

Keywords: magnetoelectric coupling, multiferroic nanocomposites, self-assembled thin film, $BiFeO_3$-$CoFe_2O_4$

*Author to whom correspondence should be addressed: guotian@m.scnu.edu.cn; caross@mit.edu; xingsengao@scnu.edu.cn;

1. Introduction

Multiferroic materials and composites combine two or more ferroic orders, such as ferroelectricity and ferromagnetism. They may furthermore show a sizeable magnetoelectric (ME) coupling, which enables a wide range of applications including actuators, logic devices, ME sensors, and nonvolatile random-access memories (RAMs).[1-6] Compared with single-phase ME materials, ME composites consisting of a ferroelectric phase and a ferromagnetic phase are of great interest for their relatively high ME coefficients and high operational temperatures. Advances in materials synthesis techniques have stimulated research on ME composites, including vertical heteroepitaxial nanocomposites (denoted as 1-3 structures)[7-14], multilayered thin films (denoted as 2-2)[15-17], heterostructured nanodots (denoted as 0-0)[18,19], and others[20-24]. Among them, self-assembled perovskite-spinel epitaxial columnar nanocomposites, such as $BiFeO_3$-$CoFe_2O_4$ (BFO-CFO), have been extensively studied. These nanocomposites exhibit large epitaxial strain at the vertical spinel-perovskite interfaces, which enable relatively high ME coupling and tunable electronic, magnetic and multiferroic properties.[25]

BFO-CFO self-assembled nanocomposites are usually epitaxially grown on (001)-oriented pseudocubic perovskite substrates, forming magnetic CFO nanopillars with square cross-sections embedded inside the BFO matrix, with [001]-oriented out-of-plane magnetic easy axis.[7,8] There are a few investigations of the effect of different substrate orientations on the structure and magnetoelectric properties. BFO-CFO nanocomposites have been grown on (110) and (111)-orientated perovskite substrates, yielding fin-shaped and triangular-shaped CFO nanostructures respectively.[26-29] We showed recently that BFO-CFO nanocomposites on a (110)-$LaAlO_3$ (LAO) substrate exhibit a thickness-dependent strain state in both CFO nanofins and BFO domains, leading to a reorientation in the easy axis of magnetization for the CFO fins from perpendicular to in-plane, as well as a thickness-dependent phase transition in the BFO matrix from a predominantly tetragonal structure at thickness of 25 nm to a rhombohedral one at 45 nm.[29] The BFO in the nanocomposite exhibits ferroelectric textures that include stripe domains and divergent patterns attributed to the strain in the

nanocomposite, but the magnetic domain states and specifically the magnetoelectric coupling between the CFO nanofins and BFO matrix have not been described.

In this work, we use probe microscopy to demonstrate an in-plane magnetic single-domain structure in the CFO nanofins as well as a sizable magnetic coupling in BFO-CFO nanocomposites grown on (110) LAO substrates. In particular, voltage-induced 180° switching of the magnetic single domains due to magnetostatic interactions can be triggered. The results provide an example of shape and orientation effects on the magnetic configuration and magnetoelectric coupling in multiferroic composites.

2. Experimental Methods

The epitaxial BFO-CFO nanocomposite thin films (~45 nm thick) with a $La_{0.33}Sr_{0.67}MnO_3$ (LSMO) bottom electrode layer (~8 nm thick) were grown on (110)-oriented LAO substrates (lattice parameter a = 0.3787 nm) by combinatorial pulsed laser deposition at 700 °C substrate temperature and 5 mTorr oxygen pressure as described previously.[29] Separate ceramic targets of BFO and CFO were alternately ablated with a KrF excimer laser (λ = 248 nm, pulse energy density = 2.6 J/cm^2) to produce sub-monolayer amounts of each material on the substrate. The number of laser pulses on the BFO and CFO targets were 200 and 50 pulses, respectively, and this process was repeated for 200 cycles. X-ray diffraction (PANalytical X′Pert PRO) was used to identify the crystal structures and interplanar spacing of BFO and CFO phases in the nanocomposite thin film.

The surface morphology and multiferroic behavior were characterized by a scanning probe microscope (MFP-3D Infinity, Asylum Research). The local piezoresponse loop measurements were carried out by fixing the position of the piezoresponse force microscopy (PFM) probe on a region of the BFO matrix and then applying a triangle-square waveform bias voltage via the conductive PFM probe (Bruker, PMV-PT). To test the magnetoelectric coupling effect, we measured the piezoresponse loops with the magnetic field applied either in-plane (up to 3 kOe) or out-of-plane (up to 1 kOe, the limit of the instrument, VFM, Asylum Research). For

characterization of electric control of magnetization, we first imaged the initial state using a magnetic force microscopy (MFM) tip (Multi75M-C, Budget Sensors), and then poled the region by applying a scanning bias voltage through the conductive PFM probe (Bruker, PMV-PT) and remeasured the MFM images.

3. Results and discussion

Figure 1a shows the morphology of a BFO-CFO nanocomposite thin film on a (110)-oriented LAO substrate visualized by atomic force microscopy (AFM), in which the elongated CFO nanofins embedded in the BFO matrix can be identified. From the AFM image, the average length and width of the CFO nanofins were 250 nm and 60 nm, respectively, and their height is 45 nm, equal to the film thickness. X-ray diffraction (XRD) shows the cube-on-cube orientation of the CFO and BFO. As shown in Figure 1b, only (*hh*0) peaks of BFO, CFO and LAO can be observed in the θ–2θ scan, which confirmed the epitaxial growth of the nanocomposites. The epitaxial structure is further confirmed by (220) reciprocal space mapping (RSM) as shown in Figure 1c. The detailed microstructure and reciprocal space maps of the BFO-CFO nanocomposites with different thickness are described in our prior work.[29] At 45 nm thickness, the BFO is predominantly rhombohedral (R-like) with a minor component of tetragonal (T-like) BFO. The T-like BFO forms in thinner films due to in-plane compressive strain from the substrate, but the R-like BFO is stabilized for films of 45 nm and above by the tensile strain at the vertical interfaces with the CFO nanofins.

The ferroelectric and magnetic domain structures of the nanocomposites were further measured by using PFM and MFM at room temperature. To demonstrate the out-of-plane polarization reversal, the BFO-CFO nanocomposite was poled by an external electric bias in which the left region within the white dashed square was poled with a voltage of +4 V, and the right region was poled with -4 V (Figure 2a,b). The dark and bright phase contrast in these regions indicates a complete reversal of the out-of-plane polarization. The well-defined piezoresponse phase-voltage hysteresis and butterfly-like amplitude-voltage loops for a randomly selected area presented in Figure 2c also indicate ferroelectric switching. (For comparison, reversal of the in-plane

components of polarization was described in ref. [29].)

The magnetic anisotropy of the CFO phase is sensitive to the shape and crystal orientation in the nanocomposites. The magnetocrystalline anisotropy difference between <001> and <110> directions is about 0.5×10^6 erg cm^{-3}, favoring magnetization along <001>. The shape anisotropy for an infinite sheet of CFO is 0.8×10^6 erg cm^{-3} based on magnetization M_s = 360 emu cm^{-3}.[27,30,31] Hence, the contribution from shape anisotropy is larger than that from magnetocrystalline anisotropy, favoring magnetization in-plane along the length of the nanofin. CFO has a large magnetostriction and the magnetoelastic anisotropy is dominant[32]: a strain as low as 0.5% yields a magnetoelastic anisotropy an order of magnitude higher than the shape and magnetocrystalline anisotropies. Bulk CFO has a lattice parameter of 0.8387 nm compared to $2a$ = 0.7574 nm for LAO, and the CFO is therefore subject to an in-plane compressive strain. The shape and magnetoelastic anisotropies favor a magnetic easy axis along the $[\bar{1}10]_{sub}$ in-plane direction (the long axis of the nanofins).

Figure 2e-f present the morphology and MFM images for the nanocomposites measured at remanence before and after applying a magnetic field. The MFM image of each nanofin shows bright and dark contrast at the ends of the nanofins characteristic of a dipole along the length of the nanofin, similar to ref. [27] and as expected from the net anisotropy. The random left-right or right-left alignment of the dipoles in the as-grown sample (measured at H = 0 Oe) are shown in Figure 2e. After applying an 8 kOe magnetic field along the $[\bar{1}10]$ in-plane direction and imaging at remanence, the dipoles are parallel (dark contrast appears at the left and white contrast at the right of each nanofin), Figure 2f. For a clearer presentation, two CFO nanofins (red dashed areas A and B) were picked out to illustrate the correspondence between the topographical location of fins and the areas of bright and dark contrast in the MFM image. One can see clearly the magnetization reversal in region B.

Hereafter, we characterize the ME coupling within the nanocomposites by using PFM to measure the piezoresponse with and without a magnetic field. After applying a magnetic field along the short axis of the nanofins (the [001] in-plane direction), an

enhancement in piezoelectric amplitude can be identified, Figure 3a. The maximum PFM amplitude and coercive voltage of the remanent state (H = 0 Oe) are ~194 pm and ~2 V, respectively. On applying an in-plane magnetic field of 3 kOe, the maximum amplitude increases to ~312 pm, while the corresponding coercive voltage decreases to ~1.3 V. These results clearly show that the ferroelectric response of the nanocomposites is significantly affected by magnetic field, indicating ME coupling between the ferroelectric BFO matrix and magnetic CFO nanofins.

To estimate the ME effect, we calculated the lateral ME coefficient α_{31} of the nanocomposites, which is given by $\alpha_{31}=V\cdot\Delta u/(u\cdot D\cdot\Delta H)$,[21] wherein V represents the driving ac voltage (1 V) required for piezoelectric vibration (~ 370 kHz resonance), u is the piezoelectric response with no magnetic field applied, i.e. 194 pm in our work, Δu is the change of piezoelectric response upon applying a magnetic field, i.e. 118 pm with a field of 3 kOe, D is the measured thickness of the nanocomposite thin film, 45 nm, and ΔH is the applied magnetic field, 3 kOe. The coefficient α_{31} is calculated to be 4.5×10^4 mV cm^{-1} Oe^{-1}, and consistent across multiple measurements at different regions. The ME coefficient α_{31} value obtained in our work is two orders of magnitude larger than that of quasi 0-3 nanocomposite films[20], and comparable to that of PZT/CFO core-shell nanofibers[21] and 0-0 type BFO/CFO heterostructured nanodots[19] calculated by similar methods.

The α_{31} values were estimated to be 1.5×10^4 mV cm^{-1} Oe^{-1} and 2.5×10^4 mV cm^{-1} Oe^{-1} for nanocomposite thicknesses of 25 nm and 75 nm, respectively, smaller than that of 45 nm-thick nanocomposites. BFO undergoes a T-R phase transition with increasing film thickness, with T-like BFO present in thinner nanocomposite films (~25 nm thickness) due to in-plane compressive strain from the substrate, while R-like BFO is present in films with thickness over 45 nm due to the relaxation of substrate strain as well as tensile strain generated from the vertical interfaces with the CFO nanofins [29]. The 45 nm thick film is near the transition making its piezoelectric behavior sensitive to the interfacial strain induced by the magnetic field, whereas in the 75 nm thick film, the CFO nanofins are more isotropic, which may decrease the ME effect. Thus, the 45

nm thickness sample showed the largest ME coefficient.

The enhancement of the ME coefficient is related to the structure and strain states of the nanocomposites on (110)-oriented LAO substrate. The [001] in-plane magnetic field is a hard axis field which rotates the magnetization away from the [$\bar{1}$10] easy axis, and is almost sufficient to saturate the magnetization along the field. For a cubic material with magnetostriction coefficients λ_{100} and λ_{111}, rotating the magnetization from [$\bar{1}$10] to [001] leads to a strain of -¾(λ_{100} + λ_{111}) along [$\bar{1}$10], -¾(λ_{100} - λ_{111}) along [110], and 3/2λ_{100} along [001]. Taking[33] $\lambda_{100} = -670\times10^{-6}$ and $\lambda_{111} = +120\times10^{-6}$, we deduce that the CFO nanofin expands along its in-plane length and to a lesser extent out-of-plane, and contracts along its short in-plane direction as the magnetization is rotated. The deformation is assumed to be transferred to the BFO, modulating its piezoresponse. We also estimate the piezoresponse coefficient d_{33} loops from the butterfly amplitude and phase hysteresis loops, as shown in Figure 3c. With the increase of the applied magnetic field, the d_{33} value increases, which also indicates an enhancement in piezoresponse amplitude. As a comparison, the effect of an easy axis magnetic field was much smaller because this does not produce deformation in the CFO.

The effect of an out-of-plane magnetic field was also examined. As shown in Figure 3d-f, the piezoelectric amplitude is slightly weakened under out-of-plane magnetic fields of 500 Oe and 1 kOe, opposite to the results obtained by applying in-plane magnetic fields. This field magnitude is insufficient to saturate the magnetization out-of-plane,[23] but if it had caused out-of-plane saturation the strain on rotating the magnetization from [$\bar{1}$10] to [110] would be -3/2λ_{111} along [$\bar{1}$10], 3/2λ_{111} along [110], and 0 along [001]. The CFO fin would therefore expand out-of-plane and contract along its in-plane length, but the deformations related to λ_{111} are smaller than the deformations for the [001] field. The much smaller strains caused by the out-of-plane field, and the smaller field magnitude, lead to a smaller modulation of the BFO strain state and a lower magnetoelectric coefficient. The ME coefficient was 1.5×10^{4} mV cm^{-1} Oe^{-1} using the same equation, about 1/3 of the magnitude obtained for a field along the [001] direction.

We now describe the reverse ME effect, namely electric field effects on the magnetic properties. We first recorded an MFM image of the nanocomposite at remanence after saturation by an out-of-plane magnetic field, then poled the sample using an external voltage, and subsequently recorded the MFM image and compared the magnetic domain orientations. Figure 4 demonstrates the AFM and MFM images taken before and after applying a voltage of + 4.5 V. The initial MFM image shows that most of the CFO fins exhibit an in-plane single domain state, similar to the domain states observed in Figure 2e. After poling, some of the MFM contrast reverses, which suggests that the magnetization of those CFO nanofins switches to the opposite direction, as shown in Figure 4b-c. Two CFO nanofins (red dashed squares) were chosen as an example; both reversed their magnetization and retain a head-to-tail orientation.

These observations confirm that the electric field is able to cause switching of the in-plane dipoles of the CFO nanofins. However, the switching is not deterministic, and not all the nanofins reverse. Of the nanofins in Figure 4a, about 1/4 of them reversed. The behavior is analogous to that observed in a BFO-CFO nanocomposite with vertical pillars of CFO and an out-of-plane easy axis, where the pillars interact magnetostatically.[11] The applied electric field causes ferroelectric switching in the BFO accompanied by a piezoelectric strain which leads to a transient change in the magnetoelastic anisotropy of the CFO. A reduction in the net anisotropy facilitates reversal of some of the nanofins under the influence of stray fields from their neighbors. The coupled switching of nanofins as shown in Figure 4 indicates that magnetostatic coupling plays an important role. Exchange coupling may also be relevant if the nanofins are in contact with each other. This mechanism does not switch the nanofins directly, but the electric field gates their response to an external (magnetostatic) field.

4. Conclusion

In summary, the magnetic domain states, multiferroic properties and magnetoelectric coupling of BFO-CFO nanocomposites grown on (110)-oriented LAO substrate were investigated. The CFO grows as fin-shaped crystals with the magnetic

easy axis parallel to the in-plane long axis, governed by the combination of shape and magnetoelastic anisotropies. By measuring the piezoresponse hysteresis loops in an applied magnetic field, we observe a considerable influence of hard-axis in-plane magnetic field on the piezoelectric properties and estimate a ME coefficient of $\alpha_{31} = 4.5 \times 10^4$ mV cm^{-1} Oe^{-1}. An out-of-plane field or an easy axis field yield weaker coupling coefficients. Conversely, applying an electric field leads to magnetic reversal of some of the CFO nanofins as a result of interparticle magnetostatic interactions. These findings provide an opportunity to obtain anisotropic magnetoelectric effects in multiferroic composites via microstructural control.

ACKNOWLEDGMENTS

The authors would like to acknowledge financial support from the National Key Research and Development Programs of China (Grant Nos. 2016YFA0201002, 2016YFA0300101), the National Natural Science Foundation of China (Grant Nos. 11674108, 51272078, 52002134), the Science and Technology Program of Guangzhou (No. 2019050001), the project for Basic and Applied Basic research Foundation of Guangdong Province (No.2019A1515110707), the Natural Science Foundation of Guangdong Province (No. 2016A030308019), the Science and Technology Planning Project of Guangdong Province (No. 2015B090927006, 2019KQNCX028), and the Natural Science Foundation of South China Normal University (No. 19KJ01). G. T gratefully acknowledges the financial support from China Scholarship Council (CSC). CR and SN acknowledge support of the National Science Foundation under awards DMR 1419807 and DMR 1911792.

DATA AVAILABILITY

The data that support the findings of this study are available from the corresponding author upon reasonable request.

References

[1] C. W. Nan, M. I. Bichurin, S. X. Dong, D. Viehland and G. Srinivasan, J. Appl. Phys. **103**, 031101 (2008).

[2] Y. J. Wang, J. F. Li and D. Viehland, Mater. Today **17**, 269-275 (2014).

[3] S. Dong, J. M. Liu, S. W. Cheong and Z. F. Ren, Adv. Phys. **64**, 519-626 (2015).

[4] G. Tian, W. D. Yang, D. Y. Chen, Z. Fan, Z. P. Hou, M. Alexe and X. S. Gao, Nat. Sci. Rev. **6**, 684-702 (2019).

[5] P. Zhao, Z. Zhao, D. hunter, R. Suchoski, C. Cao, S. Mathews, M. Wuttig and I. Takeuchi, Appl. Phys. Lett. **94**, 243507 (2009).

[6] J. M. Hu, Z. Li, L. Q. Chen and C. W. Nan, Nat. Commun. **2**, 553 (2011).

[7] H. Zheng, J. Wang, S. E. Lofland, Z. Ma, L. Mohaddes-Ardabili. T. Zhao, L. Salamanca-Riba, S. R. Shinde, S. B.Ogale, F. Bai, D. Viehland, Y. Jia, D. G. Schlom, M. Wuttig, A. Roytburd and R. Ramesh, Science **303**, 661 (2004).

[8] F. Zavaliche, T. Zhao, H. Zheng, F. Straub, M. P. Cruz, P. L. Yang, D. Hao and R. Ramesh, Nano Lett. **7**, 1586-1590 (2007).

[9] R. Comes, H. Liu, M. Khokhlov, R. Kasica, J. Lu and S. A. Wolf, Nano Lett. **12**, 2367-2373 (2012).

[10] S. M. Stratulat, X. L. Lu, A. Morelli, D. Hesse, W. Erfurth and M. Alexe, Nano Lett. **13**, 3884-3889 (2013).

[11] N. M. Aimon, D. H. Kim, X. Y. Sun and C. A. Ross, ACS App. Mater. Interfaces **7**, 2263-2268 (2015).

[12] D. H. Kim, S. Ning and C. A. Ross, J. Mater. Chem. C. **7**, 9128-9148 (2019).

[13] N, M. Aimon, H. K. Choi, X. Y. Sun, D. H. Kim and C. A. Ross, Adv. Mater. **26**, 3063-3067 (2014).

[14] Y. Sharma, R. Agarwal, L. Collins, Q. Zheng, A. V. Ievlev, R. P. Hermann, V. R. Cooper, S. KC, I. N. Ivanov, R. S. Katiyar, S. V. Kalinin, H. N. Lee, S. Hong and T. Z. Ward, Adv. Func. Mater. **30**, 1906849 (2020).

[15] M. Ghidini, F. Maccherozzi, X. Moya, L. C. Phillips, W. Yan, J. Soussi, N. Metallier, M. E. Vickers, N. J. Steinke, R. Mansell, C. H. W. Barnes, S. S. Dhesi and N. D. Mathur,

Adv. Mater. **27**, 1460-1465 (2015).

[16] H. C. He, J. Wang, J. P. Zhou and C. W. Nan, Adv. Funct. Mater. **17**, 1333-1338 (2007).

[17] J. Okabayashi, Y. Miura and T. Taniyama, npj Quantum Mater. **4**, 21 (2019).

[18] X. L. Lu, Y. Kim, S. Goetze, X. G. Li, S. Dong, P. Werner, M. Alexe and D. Hesse, Nano Lett. **11**, 3202-3206 (2011).

[19] G. Tian, F. Y. Zhang, J. X. Yao, H. Fan, P. L. Li, Z. W. Li, X. Song, X. Y. Zhang, M. H. Qin, M. Zeng, Z. Zhang, J. J. Yao, X. S. Gao and J. M. Liu, ACS Nano **10**, 1025-1032 (2016).

[20] Y. X. Li, Z. C. Wang, J. J. Yao, T. N. Yang, Z. G. Wang, J. M. Hu, C. L. Chen, R. Sun, Z. P. Tian, J. F. Li, L. Q. Chen and D. Viehland, Nat. Commun. **6**, 6680 (2014).

[21] S. H. Xie, F. Y. Ma, Y. M. Liu and J. Y. Li, Nanoscale **3**, 3152 (2011).

[22] Y. F. Wei, S. Matzen, C. P. Quinteros, T. Maroutian, G. Agnus, P. Lecoeur and B. Noheda, npj Quantum Mater. **4**, 62 (2019).

[23] X. S. Gao, B. J. Rodriguez, L. F. Liu, B. Birajdar, D. Pantel, M. Ziese, M. Alexe and D. Hesse, ACS Nano **4**, 1099-1107 (2010).

[24] H. An, H. J. Hong, Y. R. Jo, S. G. Jung, S. Kim, S. Kim, J. Lee, H. Choi, H. Yoon, S. Y. Kim, J. Song, S. Y. Jeong, B. H. Lee, T. Y. Koo, T. Park, K. T. Ko, B. Kim, B. J. Kim, C. W. Bark and S. Lee, NPG Asia Mater. **11**, 68 (2019).

[25] A. P. Chen, J. M. Hu, P. Lu, T. N. Yang, W. R. Wang, L. G. Li, T. Ahmed, E. Enriquez, M. Weigand, Q. Su, H. Y. Wang, J. L. MacManus-Driscoll, L. Q. Chen, D. Yarotski and Q. X. Jia, Sci. Adv. **2**, e1600245 (2016).

[26] D. H. Kim, J. Yang, M. S. Kim and T. C. Kim, J. Cryst. Growth **449**, 62-66 (2016).

[27] Z. G. Wang, Y. X. Li, R. Viswan, B. L. Hu, V. G. Harris, J. F. Li and D. Viehland, ACS Nano **7**, 3447-3456 (2013).

[28] L. Yan, F. Bai, J. Li and D. Viehland, J. Am. Ceram. Soc. **92**. 17 (2009).

[29] G. Tian, S. Ojha, S. Ning, X. S. Gao and C. A. Ross, Adv. Electron. Mater. **5**, 1900012 (2019).

[30] H. Zheng, J. Kreisel, Y. H. Chu, R. Ramesh, L. Salamanca-Riba, Appl. Phys. Lett.

90, 113113 (2007).

[31] G. Lavorato, E. Winkler, B. Rivas-Murias, F. Rivadulla, Phys. Rev. B **94**, 054405 (2016).

[32] G. Hu, J. H. Choi, C. B. Eom, V. G. Harris, Y. Suzuki, Phys. Rev. B **62**, R779 (2000).

[33] R.C. O'Handley, Modern Magnetic Materials, Wiley, NY (2000)

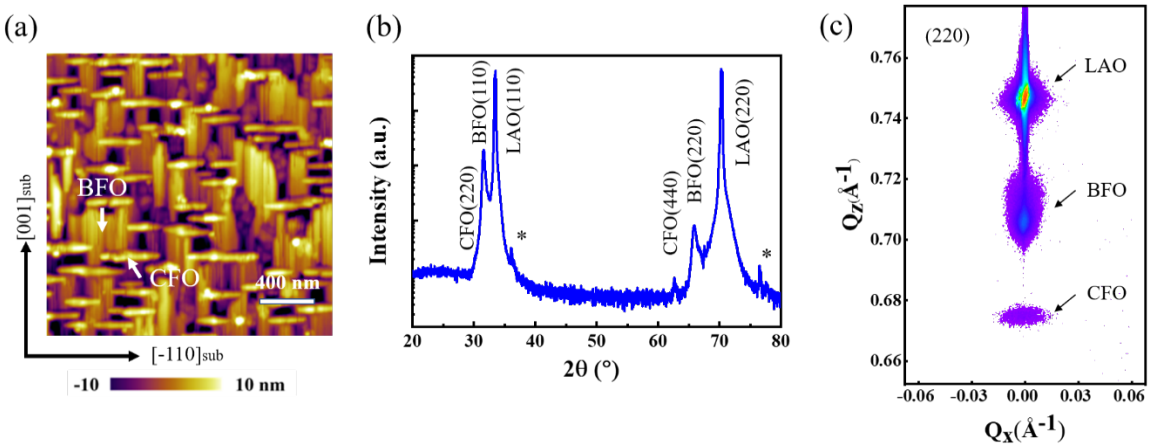

Figure 1. (a) Surface morphology, (b) θ-2θ XRD pattern of a BFO-CFO nanocomposite on (110)-LAO substrate and (c) reciprocal space mapping adjacent to the LAO (220) plane. *Additional peaks from substrate.

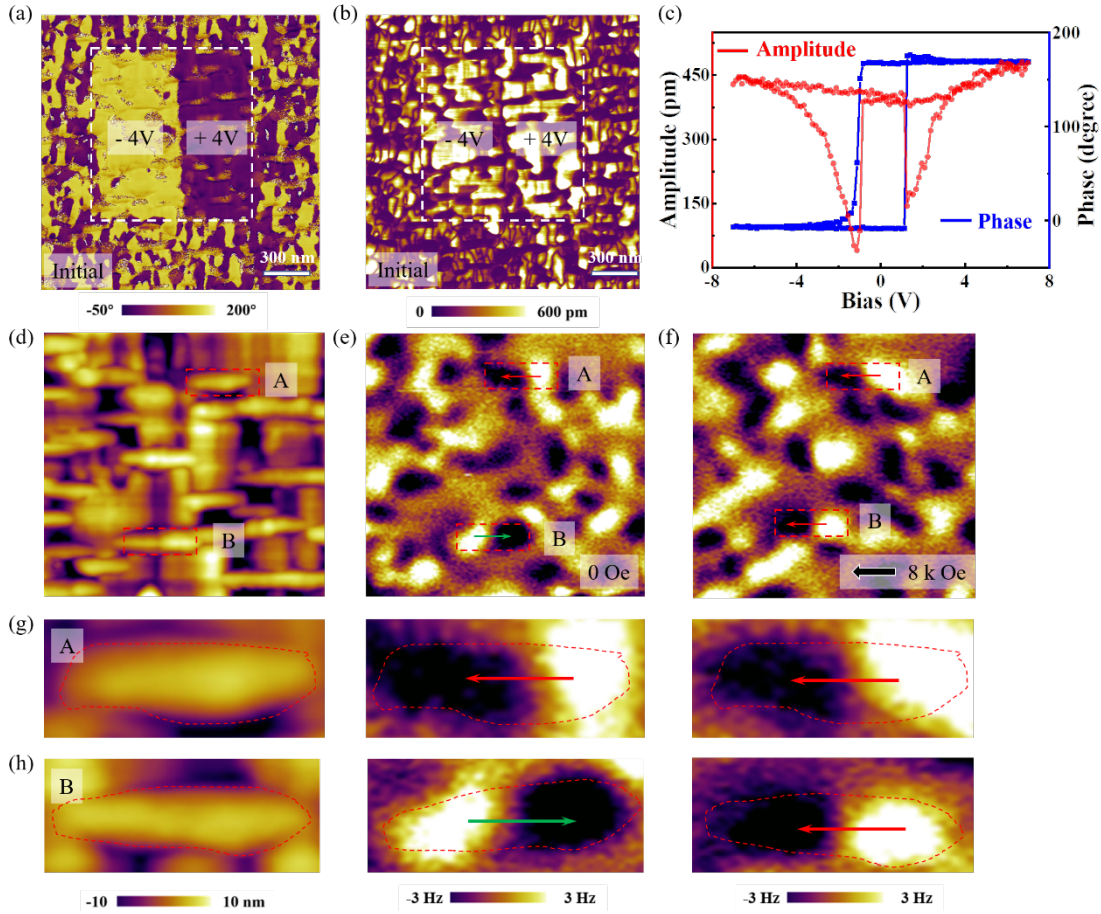

Figure 2. Ferroelectric and magnetic domains in the nanocomposites. (a-c) piezoresponse properties: vertical PFM phase (a) and amplitude (b) images, in which the middle left region was poled up with a voltage of -4 V while the middle right region was poled down with a voltage of +4 V, as well as local piezoresponse hysteresis loops (c). (d) The surface morphology, and the corresponding MFM micrograph recorded at remanence before (e) and after applying 8 kOe (f) along [$\bar{1}$10] (long axis of the nanofins). (g-h) Selected nanofins A (g) and B (h) in figure 2d-f show a correspondence between the topographical image of the nanofins and the bright and dark MFM contrast.

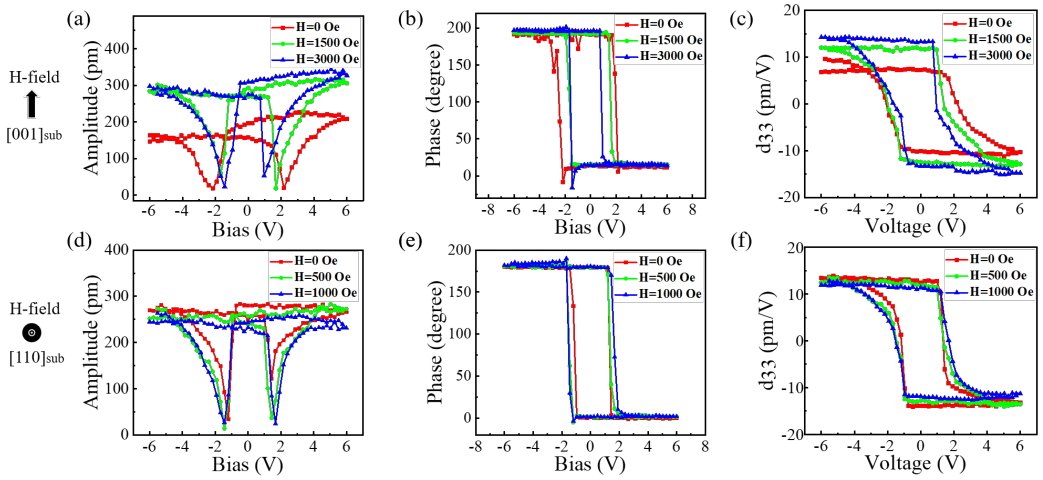

Figure 3. The piezoresponse hysteresis loops under magnetic fields along two different directions. (a-c) Butterfly shaped amplitude-voltage loops (a), phase-voltage hysteresis loops (b) and corresponding d_{33} loops (c) under three different in-plane magnetic fields (0 Oe, 1500 Oe and 3000 Oe) along the [001] in-plane direction. (d-f) Butterfly shaped amplitude-voltage loops (d), phase-voltage hysteresis loops (e) and corresponding d_{33} loops (f) under three different out-of-plane magnetic fields (0 Oe, 500 Oe and 1000 Oe) along the [110] out-of-plane direction.

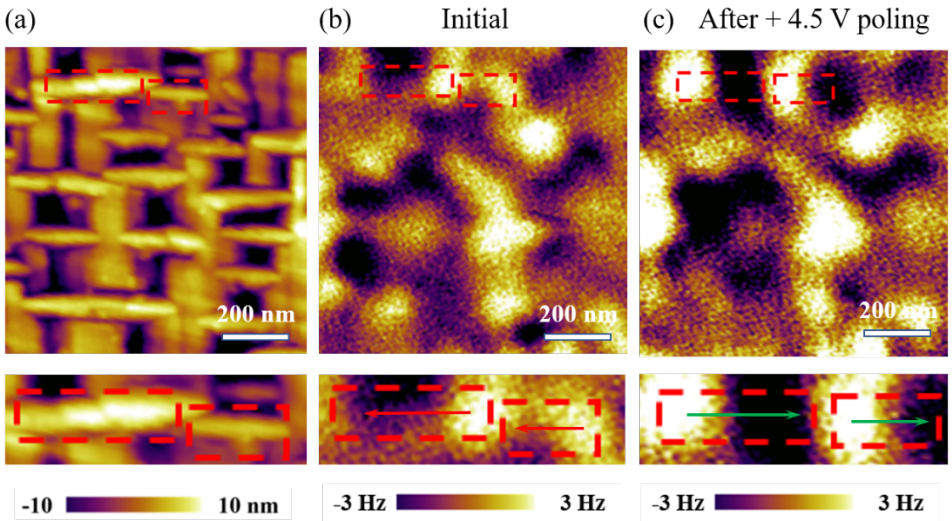

Figure 4. Electric field induced domain switching in the CFO nanofins. (a) Topographic image, (b) and the corresponding MFM images before (b) and after (c) applying a scanning external bias voltage of +4.5 V. The red dashed squares show one to one correspondence between the topographical image of fins and the corresponding bright and dark contrast in the MFM image. The lower panels show selected area magnified

images.